AGU PUBLICATIONS

JGR

Journal of Geophysical Research: Space Physics

RESEARCH ARTICLE
10.1002/2015JA021147

Key Points:
- Interplanetary shocks and solar cycle
- Statistical analysis of interplanetary shock properties
- Geomagnetic activity triggered by interplanetary shocks

Supporting Information:
- Table S1

Correspondence to:
D. M. Oliveira,
dmz224@wildcats.unh.edu

Citation:
Oliveira, D. M., and J. Raeder (2015), Impact angle control of interplanetary shock geoeffectiveness: A statistical study, *J. Geophys. Res. Space Physics*, *120*, doi:10.1002/2015JA021147.

Received 19 FEB 2015
Accepted 6 MAY 2015
Accepted article online 11 MAY 2015

Impact angle control of interplanetary shock geoeffectiveness: A statistical study

Denny M. Oliveira[1] and Joachim Raeder[1]

[1]Department of Physics and EOS Space Science Center, University of New Hampshire, Durham, New Hampshire, USA

Abstract We present a survey of interplanetary (IP) shocks using Wind and ACE satellite data from January 1995 to December 2013 to study how IP shock geoeffectiveness is controlled by IP shock impact angles. A shock list covering one and a half solar cycle is compiled. The yearly number of IP shocks is found to correlate well with the monthly sunspot number. We use data from SuperMAG, a large chain with more than 300 geomagnetic stations, to study geoeffectiveness triggered by IP shocks. The SuperMAG *SML* index, an enhanced version of the familiar *AL* index, is used in our statistical analysis. The jumps of the *SML* index triggered by IP shock impacts on the Earth's magnetosphere are investigated in terms of IP shock orientation and speed. We find that, in general, strong (high speed) and almost frontal (small impact angle) shocks are more geoeffective than inclined shocks with low speed. The strongest correlation (correlation coefficient $R = 0.78$) occurs for fixed IP shock speed and for varied IP shock impact angle. We attribute this result, predicted previously with simulations, to the fact that frontal shocks compress the magnetosphere symmetrically from all sides, which is a favorable condition for the release of magnetic energy stored in the magnetotail, which in turn can produce moderate to strong auroral substorms, which are then observed by ground-based magnetometers.

1. Introduction

Interplanetary (IP) shocks occur throughout the heliosphere as a result of the interaction of solar disturbances with the solar wind [*Burlaga*, 1971; *Richter et al.*, 1985]. In the events of IP shock interactions with the Earth's magnetosphere, IP shocks cause disturbances that can be seen throughout the magnetosphere. Some of these disturbances can have implications in several sectors of both magnetosphere and ionosphere, for example, SSCs (storm sudden commencements), geomagnetic storms, auroral substorms, and GICs (ground-induced currents). GICs may impact power grids, causing electric power disruptions due to equipment damage [*Bolduc*, 2002; *Kappenman*, 2010] and interruption of commercial activities leading to severe economic losses [*Schrijver et al.*, 2014].

Most IP shocks observed at 1 AU are fast forward shocks. Although slow shocks occur close to the Sun, a few slow shocks may be observed at Earth's orbit [*Chao and Olbert*, 1970; *Whang et al.*, 1996]. IP shocks are then classified as forward and reverse. Forward shocks propagate away from the Sun, and reverse shocks propagate toward the Sun in the solar wind frame. However, all shocks propagate in directions opposite to the Sun because the solar wind is rarely not supermagnetosonic. IP shocks may also be classified by their strength in terms of the compression ratio, the ratio between the downstream and upstream plasma density, and Mach numbers. Among other parameters, the shock normal is another important feature of IP shocks, because shock normal orientations determine how IP shocks propagate throughout the heliosphere. ICMEs (interplanetary coronal mass ejections) generally drive IP shocks whose shock normals are close to the Sun-Earth line when propagating by 1 AU [*Richter et al.*, 1985]. However, shocks may have shock normals performing large angles in relation to the Sun-Earth line. Such shocks are typically driven when the slow solar wind is compressed by the fast solar wind, or when CIRs (corotating interaction regions) take place [*Hundhaunsen*, 1972; *Pizzo*, 1991]. Calculations of IP shock normals are very sensitive to upstream and downstream plasma parameters, and using data from more than one spacecraft is thought to improve shock normal determinations [*Russell et al.*, 2000].

Here our primary concern is to study the influence of IP shock normal orientations on IP shock geoeffectiveness. Studies addressing the same shock geometry with different parameters have been reported in the past years. An example is the work of *Jurac et al.* [2002], who found that the angle between the shock normal and

the upstream magnetic field vector plays an important role in the shock geoeffectiveness. Their main result was the finding that almost perpendicular shocks were more geoeffective than quasi-parallel shocks. *Takeuchi et al.* [2002] reported the observation of an IP shock highly inclined in relation to the equatorial plane leading to an unusually SSC rise time (~30 min). They attributed this result to the fact that the IP shock observed took a longer time to sweep over what they called the "geoeffective magnetopause." By performing global MHD simulations, *Guo et al.* [2005] showed that two similar IP shocks with different shock normal orientations, namely, a frontal shock and a highly inclined shock whose shock normals lay in the equatorial plane, interacted with the magnetosphere leading to different conclusions. They reported that the inclined case took longer than the frontal case to reach fairly similar final quasi-steady states. Later on, *Wang et al.* [2006] used a shock database with Wind and ACE observations between 1995 and 2004 to study the effects of shock normal inclinations in the SSC rise time. They concluded that the SSC rise time was shorter when the shock hit the magnetopause almost head-on. When shocks hit the magnetopause with high inclination, they observed longer SSC rise time, as previously suggested by *Takeuchi et al.* [2002].

More recently, the geoeffectiveness of IP shocks controlled by IP shock impact angles was studied by *Oliveira and Raeder* [2014] through global MHD simulations. Using the Open Global Geospace Circulation Model MHD code [*Raeder*, 2003], they showed that similar IP shocks with different IP shock impact angles may lead to different IP shock geoeffectiveness. They simulated three different IP shocks, where two had shock normals inclined in relation to the Sun-Earth line in the meridian plane. The Mach number of the second shock was twice the Mach number of the first shock. Both shocks were oblique; i.e., their shock normals were at angles close to 45° with the upstream magnetic field in the shock frame of reference. Finally, in their simulations, a third perpendicular shock impacted the Earth's magnetosphere frontally, with the same Mach number of the first shock. *Oliveira and Raeder* [2014] found that the third shock was much more geoeffective than the other two because the shock was frontal, and the magnetosphere was compressed symmetrically on both north and south sides. This compression led then to the triggering of a strong auroral substorm not seen in the other cases.

The goal of this work is to confirm the role of IP shock impact angles in the IP shock geoeffectiveness using satellite and geomagnetic activity data. The geomagnetic activity triggered by such interactions is then analyzed using an enhanced version of the geomagnetic *AL* index. The data and methodology used are discussed in section 2. We present our statistical results in section 3, and we summarize and discuss our results in section 4.

2. Data and Methodology

2.1. Data

We screen solar wind plasma and field data at 1 AU to find fast forward IP shock events. In order to do so, we use two different spacecraft close to the equatorial plane: Wind, with data from 1995 up to 2013, and ACE, with data from 1998 also up to 2013. The Wind data were obtained with 93 s time resolution from the Solar Wind Experiment [*Ogilvie et al.*, 1995] and Magnetic Fields Investigation [*Lepping et al.*, 1995] instruments. The ACE data were obtained with 64 s time resolution from the Solar Wind Electron, Proton, and Alpha Monitor [*McComas et al.*, 1998; *Smith et al.*, 1998] instruments. All data were downloaded from the Coordinated Data Analysis Web (CDAWeb) interface located at http://cdaweb.gsfc.nasa.gov. All these data were used to compile a list of 461 fast forward IP shock events that can be found in the supporting information.

The monthly averaged sunspot number (SSN) data were compiled by the Solar Influence Data Analysis Center (SIDC). This list was downloaded from http://sidc.oma.be/silso/datafiles.

It is well established that substorm activity may be triggered by IP shocks [*Kokubun et al.*, 1977; *Akasofu and Chao*, 1980; *Zhou and Tsurutani*, 2001; *Yue et al.*, 2010; *Tsurutani et al.*, 2014; *Oliveira and Raeder*, 2014] and that *AL* appears to be the preferred index to quantify the strength of auroral activity [*Mayaud*, 1980]. The *AE* index, the auroral electrojet index, was first suggested by *Davis and Sugiura* [1966] and has been heavily used by magnetospheric physicists since then. However, as pointed out by *Davis and Sugiura* [1966] themselves and reviewed by *Rostoker* [1972], the indices *AU*, *AL*, and $AE = AU - AL$, available at the World Data Center in Kyoto, Japan, website (http://wdc.kugi.kyoto-u.ac.jp/aeasy/index.html), are limited because of the relatively low number of ground stations used to define these indices which happens to be 12. Therefore, it is clear that sometimes strong auroral events are underestimated because there are no ground stations under the

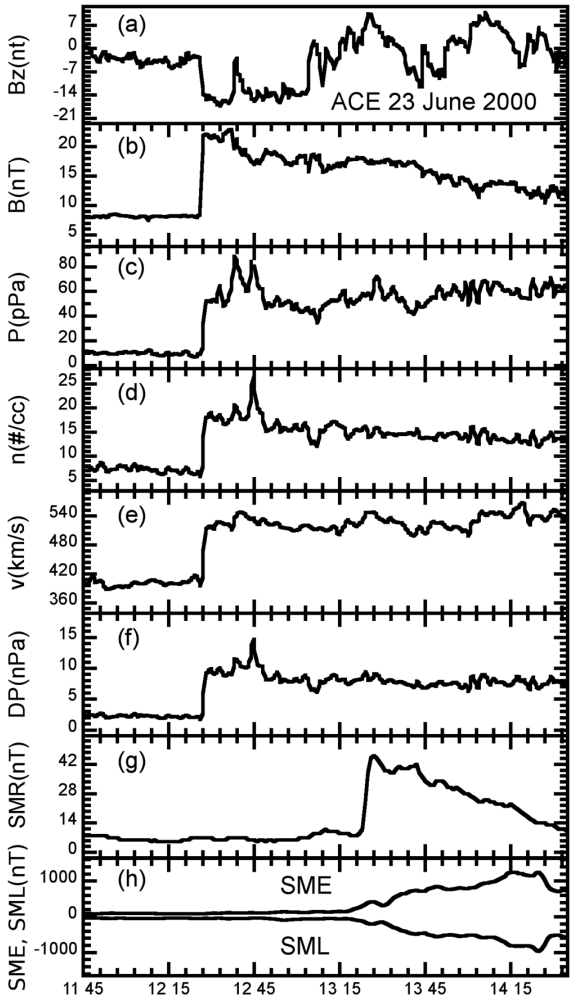

Figure 1. The IP shock event seen by ACE on 23 June 2000 at 1227 UT is an example of the methodology used for shock normal calculation and geomagnetic activity analysis. (a–f) Jumps in B_z and total magnetic field, in nT; thermal plasma pressure, in pPa; particle number density, in cm^{-3}; shock speed, in km/s; and dynamic pressure DP (ρv^2), in nPa. Figures 1g and 1h show SuperMAG data for the symmetric ring current *SMR* (similar to *SYM-H*), *SME*, and *SML*, all in nT. The maximum geomagnetic activity was recorded for both *SME* and *SML* approximately 1 h after the shock impact. The time interval used to identify peaks in geomagnetic activity for all IP shocks was 2 h after shock impacts.

auroral bulge contributing to the construction of these indices during some strong auroral substorm events [*Gjerloev et al.*, 2004]. As an alternative to alleviate this deficiency, SuperMAG, a large worldwide collaboration involving more than 300 ground-based magnetometers, was formed [*Gjerloev*, 2009]. Because the *AU*, *AL*, and *AE* indices are recognized as official indices by International Association of Geomagnetism and Aeronomy (IAGA), SuperMAG defines *SMU* as the SuperMAG measurement of the maximum eastward auroral electrojet strength (upper envelope of *N* component measured by stations between 40° and 80° magnetic north), *SML* as the SuperMAG measurement of the maximum westward auroral electrojet strength (lower envelope of *N* component measured by stations between 40° and 80° magnetic north), and $SME = SMU - SML$ as the SuperMAG measurement of the auroral electrojet index defined as the distance between the last two indices [*Newell and Gjerloev*, 2011].

An example of an auroral substorm event observed by different numbers of IAGA and SuperMAG stations is represented by Figure 1 in *Newell and Gjerloev* [2011]. In their event, it is shown by Polar Ultraviolet Imager

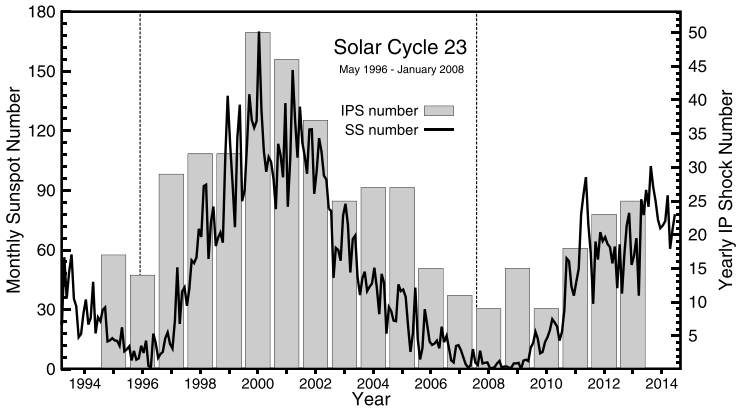

Figure 2. Yearly IP shock number (gray bars) plotted against the SIDC monthly sunspot number (solid line). Wind and ACE data were used to identify all IP shock events. A strong correlation can be seen. The maximum yearly IP shock number occurred in the year 2000 (50 events), in the solar maximum of the solar cycle 23. Due to the unusually low sunspot number in the maximum of the current solar cycle, only 25 events were observed in 2013, and not many more are expected to be identified in the 2014 and 2015 Wind and ACE data [*Smith et al.*, 2014].

(UVI) that the expansion of the auroral bulge traveled over no *AE* ground stations but instead passed over almost 10 of the *SME* ground stations. This auroral substorm was underestimated by the *AE* stations, as shown by *Newell and Gjerloev* [2011] in their Figure 2. The *AL* stations did not detect a substorm event; however, the *SML* stations recorded a substorm onset 37 s after the onset registered by Polar UVI observations. Therefore, it is important to mention that *AE* and *SME*, besides the other SuperMAG indices, are primarily of the same nature, but with the SuperMAG indices being enhanced by the higher number of ground-based stations used to build the SuperMAG indices. More details about the SuperMAG initiative can be found in *Gjerloev* [2009] and *Newell and Gjerloev* [2011], and an explanation about data techniques and assimilation is reported by *Gjerloev* [2012]. Finally, the data are available from the SuperMAG websites http://supermag.jhuapl.edu/ and http://supermag.uib.no/.

2.2. Determination of Shock Parameters and Event Analyses

IP shocks during the period investigated here have been cataloged by several sources, such as the Harvard-Smithsonian Center for Astrophysics IP shock list compiled by Dr. J. C. Kasper located at http://www.cfa.harvard.edu/shocks/wi_data/ for Wind data and http://www.cfa.harvard.edu/shocks/ac_master_data/ for ACE data. We also used a shock list compiled by the ACE team available at http://www-ssg.sr.unh.edu/mag/ace/ACElists/obs_list.html#shocks. Another source used was the shock list with only ACE data from February 1998 to August 2008 published by *Wang et al.* [2010]. All these lists were merged to compile the shock list used here. We also used an automated search program to detect IP shock candidates in the raw data. After the shock was visually inspected, and if it satisfied the Rankine-Hugoniot conditions, the event was included in our list. Other sources were also consulted for comparison among several events in terms of solar wind conditions and IP shock parameters, such as calculated IP shock normal angles and speeds, when available [*Berdichevsky et al.*, 2000; *Russell et al.*, 2000; *Zhou and Tsurutani*, 2001; *Přech et al.*, 2008; *Wang et al.*, 2009; *Richardson and Cane*, 2010; *Koval and Szabo*, 2010; *Zhang et al.*, 2012; *Grygorov et al.*, 2014].

Once a shock was identified, solar wind data from Wind and ACE were inspected to provide the basis for IP shock parameter calculations. It is well known that IP shock normal calculations are very sensitive to upstream and downstream plasma parameters. Then, the highest quality available spacecraft data were chosen for shock parameter determinations as described below. From a total of 461 identified fast forward IP shocks, 272 were observed by ACE (59%) and 189 were observed by Wind (41%).

There have been a variety of shock normal determination methods suggested since late 1960s. Some of the most commonly used methods using single spacecraft data are the magnetic and velocity coplanarity [*Colburn and Sonett*, 1966], and the mixed interplanetary magnetic field and plasma data methods [*Abraham-Shrauner*, 1972; *Abraham-Shrauner and Yun*, 1976; *Viñas and Scudder*, 1986]. Although situations

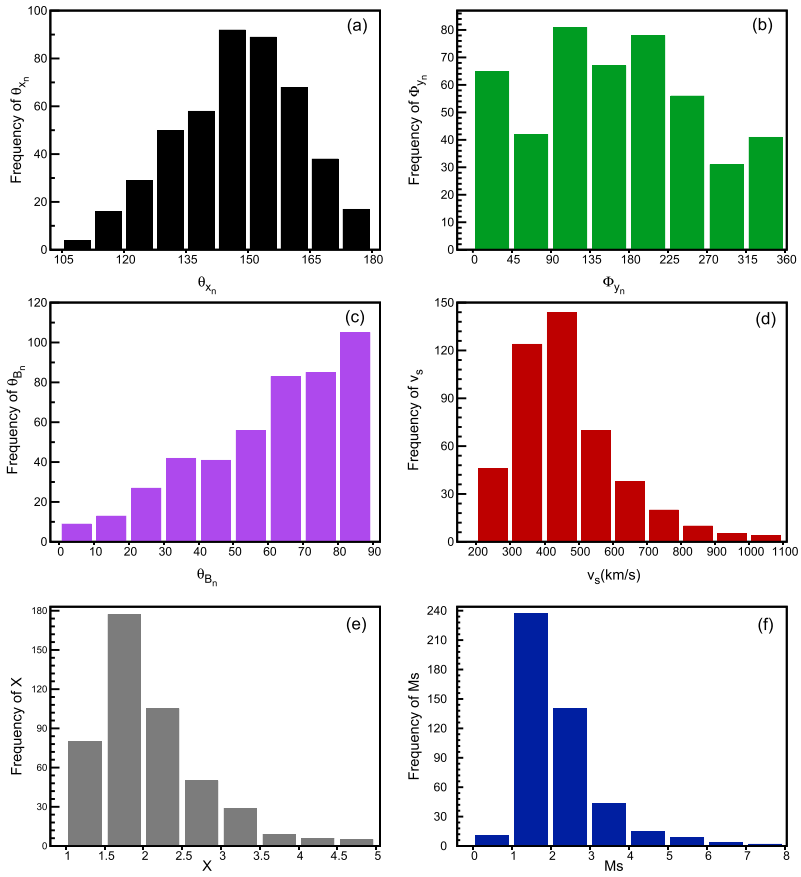

Figure 3. Statistical results of the full list with 461 IP shocks. (a) The distribution of the impact angle between the shock normal and the Sun-Earth line. Angles close to 180° represent almost frontal shocks. (b) The clock angle φ_{y_n} distribution on the GSE *YZ* plane. Angles in the ranges $0° \leq \varphi_{y_n} \leq 45°$, $135° \leq \varphi_{y_n} \leq 225°$, and $315° \leq \varphi_{y_n} \leq 360°$ indicate that the shock normals were close to the equatorial plane. (c) The distribution of θ_{B_n}, the angle between the upstream magnetic field vector and the shock normal. (d) The shock speed (in km/s) distribution, in relation to the spacecraft frame of reference. (e) The distribution of the compression ratio, the ratio of the downstream to upstream plasma densities. Finally, (f) the fast magnetosonic Mach number distribution.

where data from more than one spacecraft are available give more reliable results [*Burlaga et al.*, 1980; *Russell et al.*, 1983a, 1983b; *Russell and Alexander*, 1984; *Thomsen*, 1988; *Russell et al.*, 2000; *Szabo*, 2005; *Koval and Szabo*, 2010], we use the methods based only on one spacecraft. Multiple spacecraft data usage would create an inconsistent data set in a large statistical study, because the availability of more than one spacecraft data for shock normal determination is rare. The IP shock normals are then calculated using the methods of magnetic coplanarity, velocity coplanarity, and the three mixed plasma and field data methods found in *Schwartz* [1998]. Then, the average of the at least three closest results is calculated and registered as the chosen IP shock normal for each event.

An example of an event analysis is shown in Figure 1. This shock event was seen by ACE on 23 June 2000. At 1227 UT and (234,36.6,−0.7) R_E GSE upstream of the Earth, ACE-observed sharp jumps in magnetic field B_z component, total magnetic field, plasma thermal pressure, particle number density, plasma velocity, and dynamic pressure ρv^2 (Figures 1a–1f). Approximately 55 min later, the shock impacted the magnetopause, the magnetosphere was compressed by the shock, and an SSC was detected by SuperMAG geomagnetic stations, as can be seen in Figure 1g for the SuperMAG symmetric ring current index *SMR* [*Newell and Gjerloev*, 2012], the SuperMAG index similar to the well-known *SYM-H* index. Increases in the SuperMAG

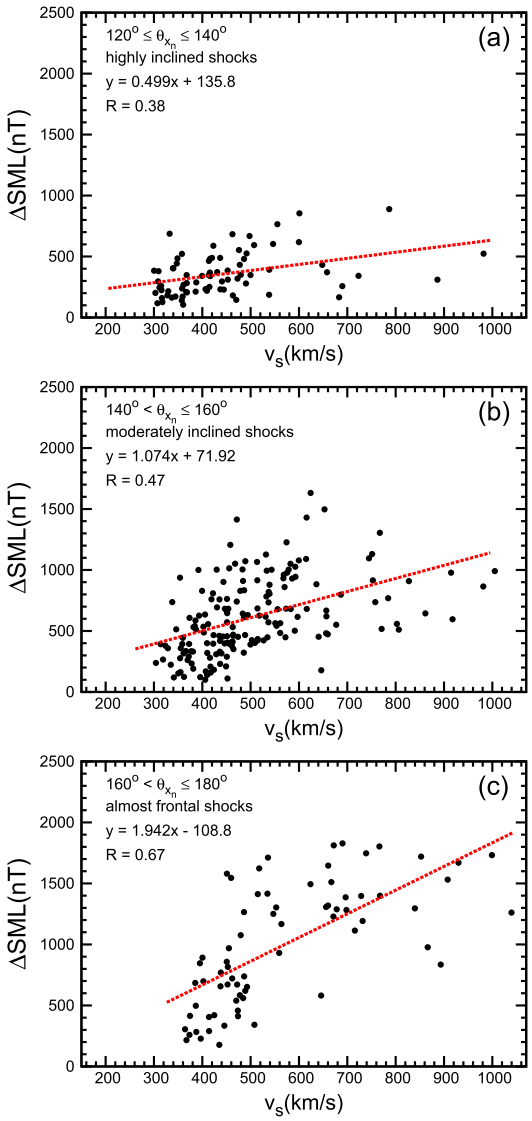

Figure 4. *SML* jumps, in nT, triggered by IP shock impacts are plotted as a function of the shock speed v_s, in km/s. The events were binned in three different groups in terms of the shock orientation in relation to the Sun-Earth line: (a) $120° \leq \theta_{x_n} \leq 140°$ (highly inclined shocks), (b) $140° < \theta_{x_n} \leq 160°$ (inclined shocks), and (c) $160° < \theta_{x_n} \leq 180°$ (almost frontal shocks). The IP shocks are more geoeffective for strong (high speed) and almost frontal shocks (large θ_{x_n}).

indices *SME* and *SML* followed the IP shock approximately 1 h after shock impact, reaching a maximum of about 1500 nT for *SME* and a minimum of about −1000 nT for *SML*. The maximum geomagnetic activity was recorded in a time lag of approximately 2 h after shock impacts for all events. Although we observed geomagnetic activity 3 h after shock impacts, we believe the time window of 2 h is enough and increasing it would not change our results significantly. This choice is consistent with time lag results reported by *Bargatze et al.* [1985], who observed that geomagnetic activity response amplitudes occurred in a time lag of 20 min due to solar wind-magnetosphere coupling and in a time lag of 60 min due to the energy release in the magnetotail. In our cases, the energy release in the magnetotail was caused by the IP shock impacts and the *SML* peaks occurred almost always more than ∼30 min after the shock impact. The calculated shock normal of this event is (−0.785, 0.153, −0.600), with θ_{x_n}∼140°, shock speed of 553.2 km/s, and fast magnetosonic Mach number 2.60. Using these results, and assuming the estimated position of the magnetopause previous to the shock impact was 10 R_E as suggested by *Zhou and Tsurutani* [1999], the calculated time travel is ∼55 min, in agreement with observations, which validates our method. To complete the shock property analysis, the compression ratio (the ratio of downstream to upstream plasma density) was 2.62, and the fast magnetosonic Mach number was 2.60.

3. Statistical Results

3.1. Solar Wind and Shock Parameters

Figure 2 shows the yearly IP shock number (gray bars) and the monthly sunspot number (SSN, solid lines) plotted in the time range from 1995 to 2013. This time period includes the whole solar cycle 23, which ranged from May 1996 to January 2008. Correlations between the number of SSCs and the SSN in different solar cycles have been reported by earlier works [*Chao and Lepping*, 1974; *Hundhaunsen*, 1979; *Smith*, 1983; *Smith et al.*, 1986; *Rastogi*, 1999]. Since most SSCs are associated with IP shocks [*Smith et al.*, 1986; *Wang et al.*, 2006],

Table 1. Summary of the Results Obtained for the Shock Speed, Shock Impact Angle, and ΔSML Correlation Analyses

Fixed Impact Angle θ_{x_n}, Changed Shock Speed v_s			
Category	Highly Inclined	Moderately Inclined	Almost Frontal
R	0.38	0.47	0.67
$\overline{\Delta SML}$ (nT)	358.4	614.0	994.7
Fixed Shock Speed v_s, Changed Impact Angle θ_{x_n}			
Category	Weak	Moderate	Strong
R	0.37	0.48	0.78
$\overline{\Delta SML}$ (nT)	388.0	684.5	955.5

these arguments are considered to be very similar. In our analysis, a correlation between both numbers is clear. During the ascending phase of the solar cycle 23, the number of IP shocks increases with the SSN. Then during the declining phase of the solar cycle 23, the number of IP shocks decreases with the SSN. *Jian et al.* [2006b] observed a higher number of coronal mass ejections (CMEs) in solar maximum in comparison to solar minimum (5 cases in 1996 and 35 cases in 2000). The CME rate was strongly correlated with solar activity. In the case of CIRs, *Jian et al.* [2006a] reported the occurrence of 17 events in 1996 and 18 events in 2000. They observed a small variation rate of CIR events with solar activity. Then, according to these results, the numbers of CIRs plus CMEs in 1996 and 2000 are, respectively, 22 and 53, which is consistent with the number of IP shocks registered in our list, 19 in 1996 and 50 in 2000. Such results indicate that IP shocks in solar minimum are more likely to be driven by CIRs, while IP shocks in solar maximum are more likely to be driven by CMEs. Due to the unusual low SSN of the current solar cycle maximum, barely more than 25 shocks are expected to be found in the Wind and ACE data for 2014 and even 2015 [*Smith et al.*, 2014].

A statistical analysis of solar wind and IP shock parameters is shown in Figures 3a–3f. Figure 3a shows θ_{x_n}, the angle between the shock normal vector and the Sun-Earth line. Angles close to 180° indicate that IP shocks were almost frontal shocks; i.e., the shock normals lay in the Sun-Earth line pointing in the direction of the Sun. IP shocks with angles close to 90° represent inclined shocks. In our list, 363 (78.57%) cases had shocks with $\theta_{x_n} \geq 135°$. The distribution of the clock angle φ_{y_n} is shown in Figure 3b. Shock normals with $0° \leq \varphi_{y_n} \leq 45°$, $135° \leq \varphi_{y_n} \leq 225°$, and $315° \leq \varphi_{y_n} \leq 360°$ indicate that the shock normal was close to the equatorial plane. These conditions were satisfied by 276 events, or 59.74%. Figure 3c shows the obliquity θ_{B_n}, the angle between the shock normal and the upstream magnetic field vector. In our data set, 354 cases showed θ_{B_n} larger than 45°, and most of the shocks in this category might have been driven by ICMEs [*Richardson and Cane*, 2010]. The shock speed distribution is shown in Figure 3d. The average shock speed is 467 km/s, and it tends to be higher in solar maximum and lower in solar minimum, as already reported by *Berdichevsky et al.* [2000] and *Echer et al.* [2003] with data partially in the same time period. The percentage of shocks above the average speed is 40.13%, or 185 events. The compression ratio, the ratio of the downstream to upstream plasma densities, can be seen in Figure 3e. As reported before [*Berdichevsky et al.*, 2000], most shocks have their compression ratios between 1.2 and 2.0, which happened to 251 of our cases (54.44%). Our compression ratio average is 2.07. Although the theoretical limit for the compression ratio is 4 [*Richter et al.*, 1985], which is derived for perpendicular shocks, this value exceeded in 11 cases (2.38%), and most of them took place slightly before and after the solar maximum (year 2000). *Echer et al.* [2003] argued that such cases can happen for some shocks in a data set in which shock obliquities range from almost parallel to almost perpendicular shocks. Finally, the fast magnetosonic Mach number distribution is shown in Figure 3f. The average of M_s is 2.15, and it is clear that most shocks have M_s between 1.0 and 3.0 [*Tsurutani and Lin*, 1985]. The number of shocks with M_s above the average is 166 (36.00%). However, some shocks have M_s less than 1, which can be an indication that such events were not shocks because the shock waves could not steepen, even though they could show some shock-like behavior [*Kennel et al.*, 1985]. These events were not included in our statistical analysis. Therefore, as a consequence of this analysis, it is possible to conclude that the interplanetary space is dominated by weak IP shocks. The agreement of our results with other works validates our statistical analysis, in particular the shock normal determination methods used in this work.

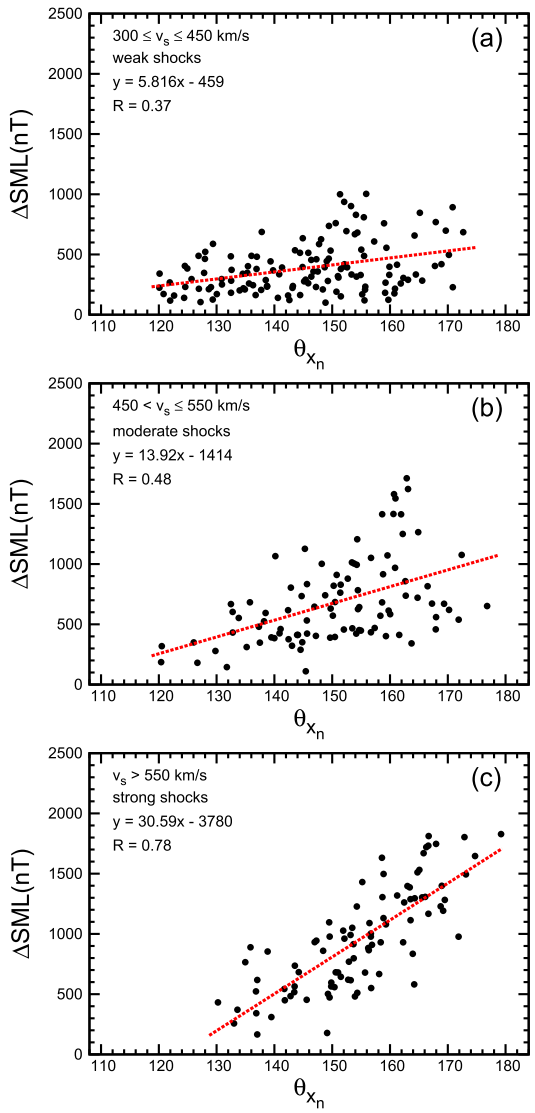

Figure 5. *SML* jumps, in nT, triggered by IP shock impacts are plotted as a function of the shock impact angle θ_{x_n}, in km/s. The events were binned in three different groups in terms of the shock speed: (a) 300 $\leq v_s \leq$ 450 km/s (weak shocks), (b) 450 $< v_s \leq$ 550 km/s (moderate shocks), and (c) $v_s >$ 550 km/s (strong shocks). The shocks are more geoeffective for almost frontal (large θ_{x_n}) and strong (high speed) IP shocks.

3.2. Geomagnetic Activity

In this section, we investigate the geoeffectiveness of IP shocks by correlating the shock parameters with the SuperMAG *SML* index as a geomagnetic activity indicator. Changes in this index, Δ*SML*, in nT, are recorded for each event in a time lag of 2 h after shock impact. If the IP shock is followed by any other solar wind structure, only the first peak in the data is considered. We chose this time frame because some inclined shocks take a long time to sweep over the magnetosphere when they are inclined in relation to the Sun-Earth line [*Takeuchi et al.*, 2002; *Guo et al.*, 2005; *Wang et al.*, 2006; *Oliveira and Raeder*, 2014]. We used SuperMAG data up to 2013 because the 2014 SuperMAG data were not yet available.

Figure 4 shows jumps in *SML*, in nT, measured by SuperMAG ground stations plotted against the shock speed, in km/s. Since we consider two parameters, shock speed and impact angle, all the data were binned in three different groups in terms of the shock normal impact angle θ_{x_n}. Here the impact angle is held and the shock speed varies. Figure 4a shows highly inclined shocks, $120° \leq \theta_{x_n} \leq 140°$; Figure 4b represents moderately inclined shocks, $140° < \theta_{x_n} \leq 160°$; and almost frontal shocks, $160° < \theta_{x_n} \leq 180°$, can be found in Figure 4c. In Figure 4a, most shocks produce little geomagnetic activity (Δ*SML* < 500 nT); and in such cases, most shocks had $v_s <$ 450 km/s. This is expected for weak and highly inclined shocks. For some stronger but highly inclined shocks, the resulting activity is slightly larger, but just a few such shocks in this case were identified in the data. The linear regression analysis gives a correlation coefficient of $R = 0.38$. In the intermediate case, i.e., the case of shocks with moderate inclination, most shocks produced Δ*SML* > 500 nT. In this case, there is a stronger correlation. We attribute the correlation coefficient of $R = 0.47$ to the fact that most shocks with $v_s <$ 450 km/s triggered small jumps in *SML* (Δ*SML* < 500 nT). For the cases in which $v_s >$ 450 km/s, Δ*SML* showed better correlations, but just a few with Δ*SML* > 1000 nT. In the more extreme case, namely, the case in which the IP shocks were almost frontal, the correlation coefficient is $R = 0.67$. In this case, approximately half of the shocks with $v_s <$ 450 km/s did not show large jumps in *SML*. Most shocks triggered Δ*SML* > 500 nT, and almost all cases in which Δ*SML* > 1000 nT had v_s larger than 450 km/s. Therefore, by inspecting all plots, it is clear that the IP shock geoeffectiveness increases with both shock strength and shock impact angle. Table 1 summarizes the results obtained in all categories in this case with the respective averages in Δ*SML* as well.

The opposite analysis is shown in Figure 5; i.e., the shock speed is held and the impact angle varies. There, ΔSML is plotted against θ_{x_n}, and the data are binned in three different categories related to the shock strength (or shock speed). Figure 5a shows the weak shocks, $300 \leq v_s \leq 450$ km/s; Figure 5b shows the moderate shocks, $450 < v_s \leq 550$ km/s; and Figure 5c shows the strong shocks, $v_s > 550$ km/s. Figure 5a shows the largest number of small ΔSML ($\Delta SML < 500$ nT), even for shocks with shock normals almost parallel to the Sun-Earth line. The correlation coefficient in this case is $R = 0.37$. A clearer $\Delta SML - \theta_{x_n}$ correlation is evident in the intermediate case, where $R = 0.48$, and most shock events have $\Delta SML > 500$ nT and $\theta_{x_n} > 135°$. All shocks with $\Delta SML > 1000$ nT had impact angles larger than 140°. In the category of strong shocks, only a few shocks triggered geomagnetic activity with $\Delta SML < 500$ nT, most of them being highly inclined shocks in which $\theta_{x_n} < 150°$. Shocks with high geoeffectiveness, or $\Delta SML > 1000$ nT, were almost frontal shocks with $\theta_{x_n} > 150°$ (only one event had θ_{x_n} slightly less than 150° in this case). The highest correlation coefficient, $R = 0.78$, occurs for IP shocks in this category. Table 1 summarizes the results obtained in all cases in this correlation analysis with the respective averages in ΔSML as well.

Thus, strong shocks are generally much more geoeffective than weak shocks, and the geoeffectiveness increases if the IP shock impacts more frontally the Earth's magnetosphere. These results have already been shown by *Wang et al.* [2006] for the SSC rise time and *Oliveira and Raeder* [2014] in global MHD simulations.

4. Summary and Conclusions

We investigated Wind and ACE solar wind data at 1 AU to compile a list of fast forward interplanetary (IP) shocks. We studied the geoeffectiveness triggered by the IP shock impacts, as measured by the jumps in the SuperMAG *SML* index, and how it relates to the shock speed (strength) and the shock inclination angles. Our main results are summarized below:

1. We provide the community with a fast forward IP shock list with events from January 1995 to December 2013, covering the whole solar cycle 23 and half of the current solar cycle.
2. The number of yearly IP shocks correlates closely with the monthly sunspot number. The highest number of fast forward IP shocks was found in the year 2000, the solar maximum of the solar cycle 23. As expected, the number of IP shocks is smaller in the maximum of the current solar cycle due to the unusual low number of sunspots occurring in this period.
3. The majority of the events (76%) is almost perpendicular shocks, with $\theta_{B_n} \geq 45°$. Most shocks (78%) have their shock normals close to the Sun-Earth line, or $\theta_{x_n} \geq 135°$. Also, less than half of the shocks (40%) have their speeds above the average of about 450 km/s, and shocks with the supermagnetosonic Mach number greater than the average 2.1 were 36%. These results indicate that the heliosphere at 1 AU is dominated by weak interplanetary shocks.
4. Strong (high speed) shocks are more geoeffective than weak shocks (low speed). The correlation is clearer when shocks are grouped in categories related to their strength and then investigated in terms of their shock impact angles. The largest correlation occurs ($R = 0.78$) when we fixed the IP shock strength, or speed, and varied the IP shock impact angles. Thus, the IP shock impact angle is just as important as their strength in determining their geoeffectiveness. This result was predicted by *Oliveira and Raeder* [2014].

Acknowledgments
This work was supported by grant NNX13AK31G from NASA, grant AGS-1143895 from the National Science Foundation, and grant FA-9550-120264 from the Air Force Office of Sponsored Research. We thank the Wind and ACE teams for the solar wind data and CDAWeb interface for data availability. We thank C.W. Smith, the ACE team, and J.C. Kasper for their list compilations. For the ground magnetometer data, we gratefully acknowledge the following: Intermagnet; USGS, Jeffrey J. Love; CARISMA, PI Ian Mann; CANMOS; The S-RAMP Database, PI K. Yumoto, and K. Shiokawa; the SPIDR database; AARI, PI Oleg Troshichev; the MACCS program, PI M. Engebretson, Geomagnetism Unit of the Geological Survey of Canada; GIMA; MEASURE, UCLA IGPP, and Florida Institute of Technology; SAMBA, PI Eftyhia Zesta; 210 Chain, PI K. Yumoto; SAMNET, PI Farideh Honary; the institutes who maintain the IMAGE magnetometer array, PI Eija Tanskanen; PENGUIN; AUTUMN, PI Martin Conners; DTU Space, PI Jrgen Matzka; South Pole and McMurdo Magnetometer, PIs Louis J. Lanzarotti and Alan T. Weatherwax; ICESTAR; RAPIDMAG; PENGUIn; British Antarctic Survey; McMac, PI Peter Chi; BGS, PI Susan Macmillan; Pushkov Institute of Terrestrial Magnetism, Ionosphere and Radio Wave Propagation (IZMIRAN); GFZ, PI Jrgen Matzka; MFGI, PI B. Heilig; IGFPAS, PI J. Reda; University of LAquila, PI M. Vellante; and SuperMAG, PI Jesper W. Gjerloev. D.M.O. thanks the SuperMAG PI J.W. Gjerloev for the straightforward SuperMAG website and its convenience of data visualization and download. The corresponding author can supply the data used in this work if contacted at dennymauricio@gmail.com.

Michael Balikhin thanks Andrey Samsonov and one anonymous reviewer for their assistance in evaluating this paper.

References

Abraham-Shrauner, B. (1972), Determination of magnetohydronamic shock normals, *J. Geophys. Res.*, *77*(4), 736–739, doi:10.1029/JA077i004p00736.

Abraham-Shrauner, B., and S. H. Yun (1976), Interplanetary shocks seen by Ames Plasma Probe on Pioneer 6 and 7, *J. Geophys. Res.*, *81*(13), 2097–2102, doi:10.1029/JA081i013p02097.

Akasofu, S.-I., and J. Chao (1980), Interplanetary shock waves and magnetospheric substorms, *Planet. Space Sci.*, *28*(4), 381–385, doi:10.1016/0032-0633(80)90042-2.

Bargatze, L. F., D. N. Baker, R. L. McPherron, and E. W. Hones Jr. (1985), Magnetospheric impulse response for many levels of geomagnetic activity, *J. Geophys. Res.*, *90*(A7), 6387–6394, doi:10.1029/JA090iA07p06387.

Berdichevsky, D. B., A. Szabo, R. P. Lepping, A. F. Viñas, and F. Mariani (2000), Interplanetary fast shocks and associated drivers observed through the 23rd solar minimum by Wind over its first 2.5 years, *J. Geophys. Res.*, *105*(A12), 27,289–27,314, doi:10.1029/1999JA000367.

Bolduc, L. (2002), GIC observations and studies in the Hydro-Québec power system, *J. Atmos. Sol. Terr. Phys.*, *64*(16), 1793–1802, doi:10.1016/S1364-6826(02)00128-1.

Burlaga, L., et al. (1980), Interplanetary particles and fields, November 22 to December 6, 1977: Helios, Voyager, and IMP observations between 0.6 and 1.6 AU, *J. Geophys. Res.*, *85*(A5), 2227–2242, doi:10.1029/JA085iA05p02227.

Burlaga, L. F. (1971), Hydromagnetic waves and discontinuities in the solar wind, *Space Sci. Rev.*, *12*(5), 600–657, doi:10.1007/BF00173345.

Chao, J. K., and R. P. Lepping (1974), A correlative study of SSC's, interplanetary shocks, and solar activity, *J. Geophys. Res.*, *79*(13), 1799–1807, doi:10.1029/JA079i013p01799.

Chao, J. K., and S. Olbert (1970), Observation of slow shocks in interplanetary space, *J. Geophys. Res.*, *75*(31), 6394–6397, doi:10.1029/JA075i031p06394.
Colburn, D. S., and C. P. Sonett (1966), Discontinuities in the solar wind, *Space Sci. Rev.*, *5*(4), 439–506, doi:10.1007/BF00240575.
Davis, T. N., and M. Sugiura (1966), Auroral electrojet activity index AE and its universal time variations, *J. Geophys. Res.*, *71*(3), 785–801, doi:10.1029/JZ071i003p00785.
Echer, E., W. D. Gonzalez, L. E. A. Vieira, A. D. L. F. L. Guarnieri, A. Prestes, A. L. C. Gonzalez, and N. J. Schuch (2003), Interplanetary shock parameters during solar activity maximum (2000) and minimum (1995–1996), *Braz. J. Phys.*, *33*(1), 115–122, doi:10.1590/S0103-97332003000100010.
Gjerloev, J. W. (2009), A global ground-based magnetometer initiative, *Eos Trans. AGU*, *90*(27), 230–231, doi:10.1029/2009EO270002.
Gjerloev, J. W. (2012), The SuperMAG data processing technique, *J. Geophys. Res.*, *117*(A9), doi:10.1029/2012JA017683.
Gjerloev, J. W., R. A. Hoffman, M. M. Friel, L. A. Frank, and J. B. Sigwarth (2004), Substorm behavior of the auroral electrojet indices, *Ann. Geophys.*, *22*(6), 2135–2149, doi:10.5194/angeo-22-2135-2004.
Grygorov, K., L. Přech, J. Šafránková, Z. Němeček, and O. Goncharov (2014), The far magnetotail response to an interplanetary shock arrival, *Planet. Space Sci.*, *103*, 228–237, doi:10.1016/j.pss.2014.07.016.
Guo, X.-C., Y.-Q. Hu, and C. Wang (2005), Earth's magnetosphere impinged by interplanetary shocks of different orientations, *Chin. Phys. Lett.*, *22*(12), 3221–3224, doi:10.1088/0256-307X/22/12/067.
Hundhaunsen, A. J. (1972), *Coronal Expansion and Solar Wind*, Springer, Berlin.
Hundhaunsen, A. J. (1979), Solar activity and the solar wind, *Rev. Geophys.*, *17*(8), 2034–2048, doi:10.1029/RG017i008p02034.
Jian, L., C. T. Russell, J. G. Luhmann, and R. M. Skoug (2006a), Properties of interplanetary coronal mass ejections at one AU during 1995–2004, *Sol. Phys.*, *239*(1–2), 393–436, doi:10.1007/s11207-006-0133-2.
Jian, L., C. T. Russell, J. G. Luhmann, and R. M. Skoug (2006b), Properties of stream interactions at one AU during 1995–2004, *Sol. Phys.*, *239*(1–2), 337–392, doi:10.1007/s11207-006-0132-3.
Jurac, S., J. C. Kasper, J. D. Richardson, and A. J. Lazarus (2002), Geomagnetic disturbances and their relationship to interplanetary shock parameters, *Geophys. Res. Lett.*, *29*(10), 1463, doi:10.1029/2001GL014034.
Kappenman, J. (2010), Geomagnetic storms and their impacts on the US power grid, *Tech. Rep.*, Metatech Corp., Goleta, Calif.
Kennel, C. F., J. P. Edmiston, and T. Hada (1985), A quarter century of collisionless shock research, in *Collisionless Shocks in the Heliosphere: A Tutorial Review*, edited by R. G. Stone and B. Tsurutani, pp. 1–36, AGU, Washington, D. C., doi:10.1029/GM034p0001.
Kokubun, S., R. L. McPherron, and C. T. Russell (1977), Triggering of substorms by solar wind discontinuities, *J. Geophys. Res.*, *82*(1), 74–86, doi:10.1029/JA082i001p00074.
Koval, A., and A. Szabo (2010), Multispacecraft observations of interplanetary shock shapes on the scales of the Earth's magnetosphere, *J. Geophys. Res.*, *115*(A12105), doi:10.1029/2010JA015373.
Lepping, R., et al. (1995), The WIND magnetic field investigation, *Space Sci. Rev.*, *71*(1–4), 207–229, doi:10.1007/BF00751330.
Mayaud, P. N. (1980), The AU, AL and AE indices, in *Derivation, Meaning, and Use of Geomagnetic Indices*, vol. 22, edited by P. N. Mayaud, pp. 96–115, AGU, Washington, D. C., doi:10.1002/9781118663837.ch7.
McComas, D., S. Bame, P. Barker, W. Feldman, J. Phillips, P. Riley, and J. Griffee (1998), Solar Wind Electron Proton Alpha Monitor (SWEPAM) for the Advanced Composition Explorer, *Space Sci. Rev.*, *86*(1–4), 563–612, doi:10.1023/A:1005040232597.
Newell, P. T., and J. W. Gjerloev (2011), Evaluation of SuperMAG auroral electrojet indices as indicators of substorms and auroral power, *J. Geophys. Res.*, *116*, A12211, doi:10.1029/2011JA016779.
Newell, P. T., and G. W. Gjerloev (2012), SuperMAG-based partial ring current indices, *J. Geophys. Res.*, *117*, A05215, doi:10.1029/2012JA017586.
Ogilvie, K., et al. (1995), SWE, a comprehensive plasma instrument for the WIND spacecraft, *Space Sci. Rev.*, *71*(1–4), 55–77, doi:10.1007/BF00751326.
Oliveira, D. M., and J. Raeder (2014), Impact angle control of interplanetary shock geoeffectiveness, *J. Geophys. Res. Space Physics*, *119*, 8188–8201, doi:10.1002/2014JA020275.
Pizzo, V. J. (1991), The evolution of corotating stream fronts near the ecliptic plane in the inner solar system: 2. Three-dimensional tilted-dipole fronts, *J. Geophys. Res.*, *96*(A4), 5405–5420, doi:10.1029/91JA00155.
Přech, L., Z. Němeček, and J. Šafránková (2008), Response of magnetospheric boundaries to the interplanetary shock: THEMIS contribution, *Geophys. Res. Lett.*, *35*, L17S02, doi:10.1029/2008GL033593.
Raeder, J. (2003), Global magnetohydrodynamics: A tutorial review, in *Space Plasma Simulation*, edited by J. Buchner, C. T. Dum, and M. Scholer, Springer, Berlin, doi:10.1007/3-540-36530-311.
Rastogi, R. G. (1999), Signatures of storm sudden commencements in geomagnetic H, Y and Z fields at Indian observatories during 1958–1992, *Adv. Space Res.*, *17*, 1426–1438, doi:10.1007/s00585-999-1426-1.
Richardson, I. G., and H. V. Cane (2010), Interplanetary circumstances of quasi-perpendicular interplanetary shocks in 1996–2005, *J. Geophys. Res.*, *115*, A07103, doi:10.1029/2009JA015039.
Richter, A. K., K. C. Hsieh, A. H. Luttrell, E. Marsch, and R. Schwenn (1985), Review of interplanetary shock phenomena near and within 1 AU, in *Collisionless Shocks in the Heliosphere: Reviews of Current Research*, edited by B. T. Tsurutani and R. G. Stone, pp. 33–50, AGU, Washington, D. C., doi:10.1029/GM035p0033.
Rostoker, G. (1972), Geomagnetic indices, *Rev. Geophys.*, *10*(4), 935–950, doi:10.1029/RG010i004p00935.
Russell, C. T., and C. J. Alexander (1984), Multiple spacecraft observations of interplanetary shocks: Shock-normal oscillations and their effects, *Adv. Space Res.*, *4*(2–3), 277–282, doi:10.1016/0273-1177(84)90321-1.
Russell, C. T., J. T. Gosling, R. D. Zwickl, and E. J. Smith (1983a), Multiple spacecraft observations of interplanetary shocks: ISEE three-dimensional plasma measurements, *J. Geophys. Res.*, *88*(A12), 9941–9947, doi:10.1029/JA088iA12p09941.
Russell, C. T., M. M. Mellott, E. J. Smith, and J. H. King (1983b), Multiple spacecraft observations of interplanetary shocks: Four spacecraft determination of shock normals, *J. Geophys. Res.*, *88*(A6), 4739–4748, doi:10.1029/JA088iA06p04739.
Russell, C. T., et al. (2000), The interplanetary shock of September 24, 1998: Arrival at Earth, *J. Geophys. Res.*, *105*(A1), 25,143–25,154, doi:10.1029/2000JA900070.
Schrijver, C. J., R. Dobbins, W. Murtagh, and S. M. Petrinec (2014), Assessing the impact of space weather on the electric power grid based on insurance claims for industrial electrical equipment, *Space Weather*, *12*, 487–498, doi:10.1002/2014SW001066.
Schwartz, S. J. (1998), Shock and discontinuity normals, Mach numbers, and related parameters, in *Analysis Methods for Multi-Spacecraft Data, ISSI Sci. Rep.*, vol. 1, edited by G. Paschmann and P. W. Daly, pp. 249–270, ESA Publ. Div., Noordwijk, Netherlands.
Smith, C., J. L'Heureux, N. Ness, M. Acuña, L. Burlaga, and J. Scheifele (1998), The ACE magnetic fields experiment, *Space Sci. Rev.*, *86*(1–4), 613–632, doi:10.1023/A:1005092216668.

Smith, C. W., K. G. McCracken, N. A. Schwadron, and M. L. Goelzer (2014), The heliospheric magnetic flux, solar wind proton flux, and cosmic ray intensity during the coming solar minimum, *Space Weather*, *12*, 499–507, doi:10.1002/2014SW001067.

Smith, E. J. (1983), Observations of interplanetary shocks: Recent progress, *Space Sci. Rev.*, *34*(1), 101–110, doi:10.1007/BF00221200.

Smith, E. J., J. A. Slavin, R. D. Zwickl, and S. J. Bame (1986), Shocks and storm sudden commencements, in *Solar Wind and Magnetosphere Coupling*, edited by Y. Kamide and J. A. Slavin, pp. 345–365, Terra Sci., Tokyo.

Szabo, A. (2005), Multi-spacecraft observations of interplanetary shocks, in *4th Annual IGPP International Astrophysics Conference on the Physics of Collisionless Shocks*, edited by G. Li, G. Zank, and C. T. Russell, pp. 37–41, AIP Conf. Proc., Am. Inst. of Phys., Washington, D. C., doi:10.1063/1.2032672.

Takeuchi, T., C. T. Russell, and T. Araki (2002), Effect of the orientation of interplanetary shock on the geomagnetic sudden commencement, *J. Geophys. Res.*, *107*(A12), 1423, doi:10.1029/2002JA009597.

Thomsen, M. F. (1988), Multi-spacecraft observations of collisionless shocks, *Adv. Space Res.*, *8*(9–10), 157–166, doi:10.1016/0273-1177(88)90126-3.

Tsurutani, B. T., and R. P. Lin (1985), Acceleration of >47 keV ions and >2 keV electrons by interplanetary shocks at 1 AU, *J. Geophys. Res.*, *90*(A1), 1–11, doi:10.1029/JA090iA01p00001.

Tsurutani, B. T., E. Echer, K. Shibata, O. P. Verkhoglyadova, A. J. Mannucci, W. D. Gonzalez, J. U. Kozyra, and M. Pätzold (2014), The interplanetary causes of geomagnetic activity during the 7–17 March 2012 interval: A CAWSES II overview, *J. Space Weather Space Clim.*, *4*, A02, doi:10.1051/swsc/2013056.

Viñas, A. F., and J. D. Scudder (1986), Fast and optimal solution to the "Rankine-Hugoniot" problem, *J. Geophys. Res.*, *91*(A1), 39–58, doi:10.1029/JA091iA01p00039.

Wang, C., C. X. Li, Z. H. Huang, and J. D. Richardson (2006), Effect of interplanetary shock strengths and orientations on storm sudden commencement rise times, *Geophys. Res. Lett.*, *33*, L14104, doi:10.1029/2006GL025966.

Wang, C., J. B. Liu, H. Li, Z. H. Huang, J. D. Richardson, and J. R. Kan (2009), Geospace magnetic field responses to interplanetary shocks, *J. Geophys. Res.*, *114*, A05211, doi:10.1029/2008JA013794.

Wang, C., H. Li, J. D. Richardson, and J. R. Kan (2010), Interplanetary shock characteristics and associated geosynchronous magnetic field variations estimated from sudden impulses observed on the ground, *J. Geophys. Res.*, *115*, A09215, doi:10.1029/2009JA014833.

Whang, Y. C., J. Zhou, R. P. Lepping, and K. W. Ogilvie (1996), Interplanetary slow shock observed from WIND, *Geophys. Res. Lett.*, *23*(10), 1239–1242, doi:10.1029/96GL01358.

Yue, C., Q. G. Zong, H. Zhang, Y. F. Wang, C. J. Yuan, Z. Y. Pu, S. Y. Fu, A. T. Y. Lui, B. Yang, and C. R. Wang (2010), Geomagnetic activity triggered by interplanetary shocks, *J. Geophys. Res.*, *115*, A00I05, doi:10.1029/2010JA015356.

Zhang, H., D. G. Sibeck, Q.-G. Zong, J. P. McFadder, D. Larson, K.-H. Glassmeier, and V. Angelopoulos (2012), Global magnetosphere response to an interplanetary shock: THEMIS observations, *Ann. Geophys.*, *30*(2), 379–387, doi:10.5194/angeo-30-379-2012.

Zhou, X., and B. T. Tsurutani (2001), Interplanetary shock triggering of nightside geomagnetic activity: Substorms, pseudobreakups, and quiescent events, *J. Geophys. Res.*, *106*(A9), 18,957–18,967, doi:10.1029/2000JA003028.

Zhou, X.-Y., and B. T. Tsurutani (1999), Rapid intensification and propagation of the dayside aurora: Large scale interplanetary pressure pulses (fast shocks), *Geophys. Res. Lett.*, *26*(8), 1097–1100, doi:10.1029/1999GL900173.